The Rosseland Mean Opacity of a Mixture of Gold and Gadolinium at High Temperatures

T. J. Orzechowski, M. D. Rosen, H. N. Kornblum, J. L. Porter,* L. J. Suter,
A. R. Thiessen, and R. J. Wallace

Lawrence Livermore National Laboratory, P.O. Box 808, Livermore, California 94550

Radiation transport through high-opacity materials can be described using the Rosseland mean opacity of the medium, which is dominated by low-opacity regions in the frequency-dependent opacity. By mixing gold and gadolinium, we can fill in low-opacity regions of one material with high-opacity regions of another material, resulting in a material with a Rosseland mean opacity $1.5\times$ higher than either of the constituents. For a given laser energy, this can raise the temperature of the laser heated hohlraums, or for a given desired temperature, require less laser energy. [S0031-9007(96)01422-6]

In the indirect drive approach [1] to inertial confinement fusion [2] the radiation that drives the implosion of the fuel capsule is generated by the interaction of intense beams, either lasers [3] or particles [4], with the interior walls of a high-Z cavity, or hohlraum. This radiation is typically described by a blackbody spectrum with a temperature of about 250 eV. This high temperature radiation not only drives the fuel pellet compression, but also heats and ablates the hohlraum wall. The interaction of the radiation with the hohlraum wall is characterized by multiple absorption and reemission of the x rays [5–7]. The ratio of the reemitted flux to the incident flux is referred to as the albedo α. The efficiency with which the radiation couples to the capsule depends on the albedo; increasing the albedo improves the coupling efficiency. The incident flux is the sum of the reemitted flux plus the x-ray flux lost to the wall. This flux lost to the wall propagates through the wall in the form of a (diffusive) ablative heat wave [8]. The rate of diffusion is (approximately) inversely proportional to the square root of the Rosseland mean opacity. Increasing the Rosseland mean opacity reduces the radiation energy lost to the walls and thus increases the albedo. Hence for a given laser power (and x-ray conversion efficiency) the drive temperature increases as does the coupling efficiency of the radiation to the fuel pellet.

The Rosseland mean opacity [9] is used to describe radiation transport in optically thick materials when the matter and radiation are in thermodynamic equilibrium. It is defined as a weighted harmonic mean of the energy dependent opacity:

$$\frac{1}{\kappa_R} \equiv \frac{\int_0^\infty \kappa_\nu^{-1}(\partial B_\nu/\partial T)\, d\nu}{\int_0^\infty (\partial B_\nu/\partial T)\, d\nu}. \tag{1}$$

Here T is the radiation and material temperature, B_ν is the blackbody spectrum, and κ_ν is the frequency-dependent opacity. This mean opacity is dominated by the regions of low opacity in the frequency-dependent opacity.

Typically we use pure Au hohlraums, heated to a temperature of $\sim$250 eV. An energy-dependent opacity for Au at a density and temperature relevant to these experiments is shown in Fig. 1. This opacity was calculated using a very simple average atom model [10] for Au at 1.0 g/cm^3 and a temperature of 250 eV. There are significant windows in the opacity at energies around the peak of the blackbody spectrum. The gross structure of the opacity shown in Fig. 1 is dominated by the bound-free (photoelectric) absorption coefficient: the sharp increases in opacity correspond to the photoionization of the various atomic shells ($K, L, M, \ldots$). Also shown in Fig. 1 is the weighting function $\partial B_\nu/\partial T$ for a 250-eV blackbody distribution. As can be seen in the figure, the peak of the weighting function is fairly broad, and the integrand of Eq. (1) reaches its maximum at an energy corresponding to the minimum in the opacity between the N- and O-band absorption edges. In order to improve the efficiency of the hohlraum we need to blend in materials whose high-opacity regions compliment the low-opacity regions of the original material. Figure 1 also shows the calculated energy-dependent opacity for gadolinium, which was chosen because its regions of high opacity occur around the same energies as the holes in the Au opacity. For this model, the Rosseland mean opacity for Au is 823 cm^2/g, for gadolinium it is 455 cm^2/g, and for a 50/50 mixture of gold and gadolinium it is

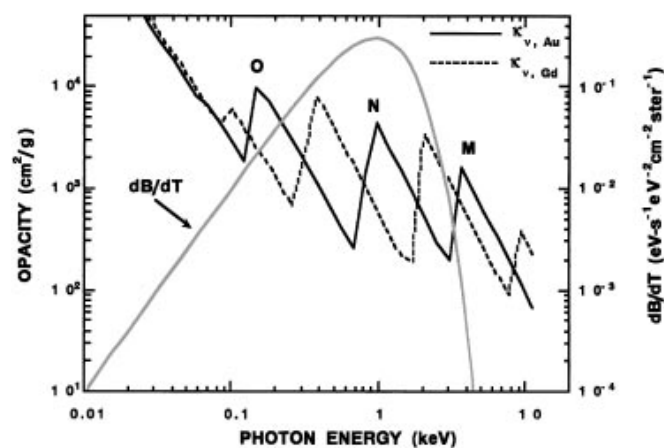FIG. 1. Frequency dependent opacity of Au and Gd. Also shown is the weighting function $(\partial B/\partial T)$ corresponding to a 250-eV Planckian distribution.

1390 cm^2/g. A more sophisticated opacity model (XSN) [11], in which bound-bound transitions play a more central role in determining opacity, gives $\kappa_R = 1500$ cm^2/g for Au, 1300 cm^2/g for Gd, and 2500 cm^2/g for the 50/50 Au/Gd mixture.

In order to determine the Rosseland mean opacity of a material, we measure the propagation time of a radiation heat wave (also referred to as a Marshak wave) through a well characterized sample of that material and compare the measurement to analytic and numerical solutions [12–14]. The nonlinear diffusion equation that governs the Marshak wave behavior includes the specific energy density and the Rosseland mean opacity of the material. Using the XSN opacity model [11], the Rosseland mean opacity for Au in the temperature range of 100 to 300 eV is found to be $\kappa = \kappa_0 \rho^{0.33} T^{-1}$, where κ is in units of cm^2/g, and κ_0 is 3500 when ρ is in g/cm^3, and T is in heV (10^2 eV). The specific energy density of the material is approximated as $\varepsilon \approx \varepsilon_0 T^{1.5}$. With these analytic models for κ and ε, the self-similar solution for the diffusion equation gives the energy lost to the wall and the position of the nonlinear Marshak wave front as a position of time [6]:

$$E_W \propto T^{3.0} t^{0.62} \kappa_0^{-0.4}, \tag{2}$$

$$\rho X_M \propto T^{1.7} t^{0.55} \kappa_0^{-0.45}. \tag{3}$$

These solutions were derived for a boundary temperature T that is constant in time. In a more general case the boundary temperature itself can vary in time, thus changing the temporal dependence of E_W and ρX_M. For example, in the case of a constant x-ray flux on the wall, $\dot{E}_W = $ const $\times$ ($\sim t^0$) and from Eq. (2) we would have the temperature scaling as $T \sim t^{0.12}$. In this case the position of the Marshak wave would scale as $t^{0.78}$. This is the sort of behavior one would expect for a constant laser power and a constant x-ray conversion efficiency. In fact, the x-ray conversion efficiency increases slowly in time: we will assume that $\eta_{CE} \sim t^{0.2}$. (Measurements from Au disks [15] using 3-ns long laser pulses indicate it could vary as $\sim t^{0.4}$. Simulations indicate a time dependence in a hohlraum of about $t^{0.12}$. The $t^{0.2}$ dependence that we chose gives the best match to the experimentally measured time dependence of the hohlraum temperature.) Using this temporal behavior for the x-ray flux (and hence wall loss), we find the temperature to scale as $t^{0.18}$ and the Marshak wave position to scale almost linearly with time:

$$\rho X_M \propto t^{0.9} \kappa_0^{-0.45}. \tag{4}$$

This time dependence of the Marshak wave position is very close to that observed experimentally [13] for Au foils of varying thickness exposed to the same hohlraum drive used in these experiments ($\rho X_M \propto t$). Also, as we shall see below, the $t^{0.18}$ dependence of the hohlraum temperature is close to that observed experimentally. Hence, this model is probably the best representation of the experiment described here.

To measure the propagation of the heat wave through a given material, we expose the sample to the near Planck-

ian radiation distribution generated inside a standard Nova hohlraum [16]. The hohlraum is driven with about 27 kJ of 351-nm radiation in a 1-ns long pulse. The experimental arrangement is shown schematically in Fig. 2. The time-dependent hohlraum temperature is monitored with an absolutely calibrated multiple-channel soft x-ray spectrometer DANTE [17]. In Fig. 2 we show the temporal profile of the total laser power and the hohlraum temperature. The laser pulse rises rather sharply ($\sim$100 ps) and exhibits a small oscillation ($\pm5\%$) during the "flat-top" region of the pulse. The corresponding hohlraum temperature rises more slowly, reaching a temperature of about 200 eV at 300 ps. Beyond this point the hohlraum temperature rises more slowly with time ($\sim t^{0.15}$) during the nominal constant laser power. This is very close to the time dependence of the temperature associated with Eq. (4). The test sample package covers a 600-μm high, 1200-μm long slot that is cut in the hohlraum wall and is centered about the hohlraum midplane. Various test materials cover portions of this slot with one section left uncovered to provide a fiducial signal at $t = 0$ (the
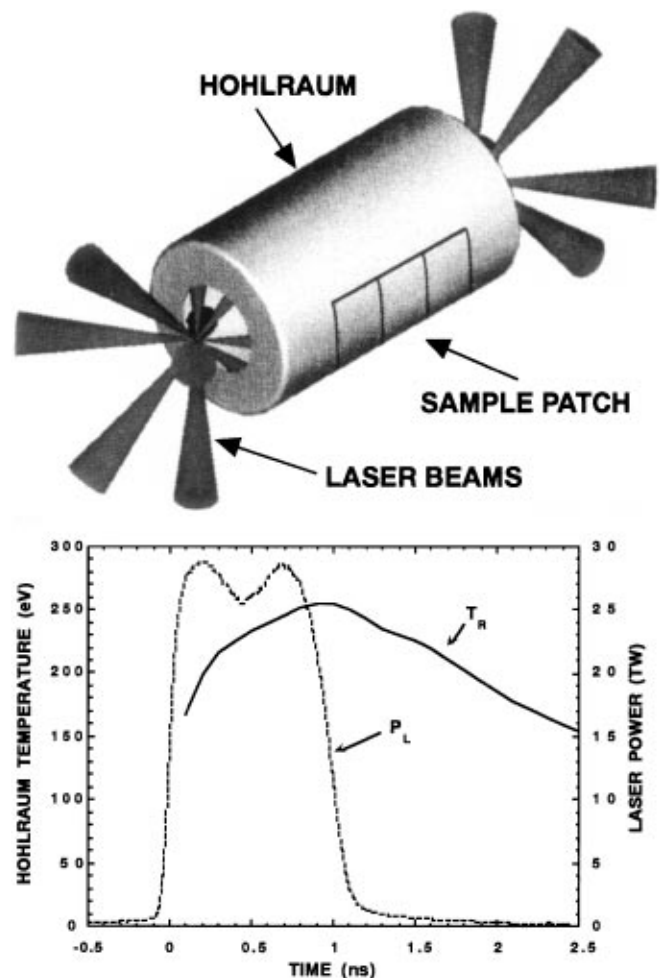

FIG. 2. Above: schematic of the hohlraum showing laser entrance holes on each end and test-sample patch fixed to the hohlraum side. Below: typical 1-ns "square" laser pulse used to drive the hohlraum and measured hohlraum temperature.

beginning of the drive pulse). The radiation inside the hohlraum drives the Marshak wave into the material. The samples are usually on the order of 1 to a few microns thick so that the radiation propagates through the sample before the drive (i.e., the laser beams) turns off.

In the measurements described here, we investigate the transport of the thermal wave through pure Au foils and gold-gadolinium mixtures. In this experiment, the Au/Gd samples are formed by depositing alternate layers of the two elements on a substrate that is later removed to provide a freestanding sample. The areal density of each layer must be optically thin to the radiation so that the radiation samples both elements simultaneously and averages over the opacity of two elements. Two different samples corresponding to different atomic fractions of Au and Gd were fabricated. One sample comprises 200 layer pairs of Au and Gd. The thickness of each layer (Au or Gd) is 75 Å. This sample is 33% Gd and 67% Au by atom. The overall thickness is 2.22 μm and the areal density of this sample is 3.15 mg/cm^2. The second sample comprises 146 layer pairs, the thickness of each Au layer is 35 Å, and the thickness of each Gd layer is 116 Å. In this case the sample is 67% Gd and 33% Au. The overall thickness of this second sample is 3.02 μm, with an areal mass of 2.97 mg/cm^2. In either of these samples, the individual thickness of each layer of either the Au or the Gd is much less than the range of a photon (100–1000 eV) in these materials. For example, the cold opacity of Au to x rays between 100 and 1000 eV is between 0.5×10^4 and 1.5×10^4 cm^2/g. For solid density, then, the range of a photon is $(\kappa\rho)^{-1}$ or about 1000 Å—much larger than the typical layer thickness ($\sim 10^2$ Å) and much less than the typical sample thickness ($\sim 10^4$ Å).

The thermal radiation corresponding to the hohlraum drive is monitored with a streaked x-ray imager (SXI) as a function of time as it burns through the different foils. The SXI images the foil in one direction using a 20-μm wide slit. The image is dispersed with a transmission grating oriented perpendicular to the imaging slit, and the energy at which we monitor the burnthrough is determined with an offset aperture located behind the transmission grating. All of the data shown here correspond to 225 eV radiation. The one-dimensional image is monitored with an x-ray streak camera. A typical image of the burnthrough patch is shown in Fig. 3. In this image, the Au/Gd foil is located on the right and the pure Au foil is located on the left. The fiducial (straight through) is located at the center of the test-sample patch and the foils are located on either side of the hohlraum midplane. The purpose of mounting the foils symmetrically about the midplane (and the fiducial) is to mitigate any possible effects of hohlraum temperature nonuniformity in the axial direction (i.e., higher hohlraum temperature closer to the laser spots).

In order to determine the ratio of the Rosseland mean opacity of the mixture to that of Au we used the results of self-similar solutions [Eq. (4)]. The ratio of the Rosseland mean opacities then depends on the ratio of the burn-
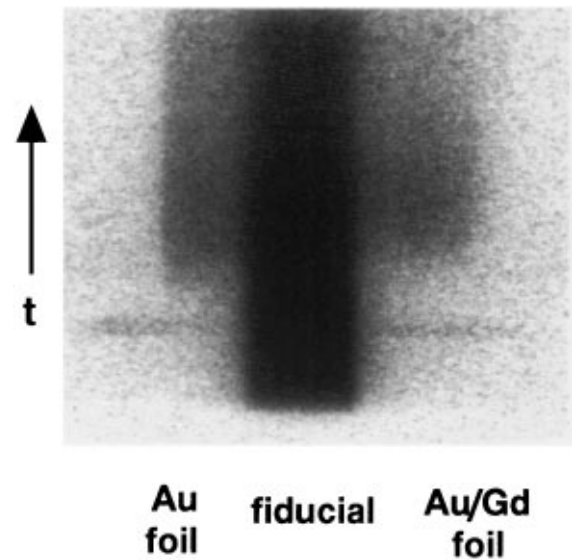

FIG. 3. Streaked image of test-sample patch monitored at 225 eV. The fiducial signal is in the center of the image, the radiation burning through the pure Au sample is on the left, and through the Au/Gd composite sample is on the right.

through times squared and the ratio of the areal masses of the foils to the 2.2 power. While the latter ratio was designed to be one, the actual values were used to determine the ratio of opacities. Figure 4 shows the ratio of the Rosseland mean opacities of the Au/Gd foil to that of Au for the two different concentrations of Gd. The errors associated with the measurement correspond to uncertainties in the streak camera sweep speed (± 15 ps) and in errors in determining the precise thickness of the foils (± 250 Å).
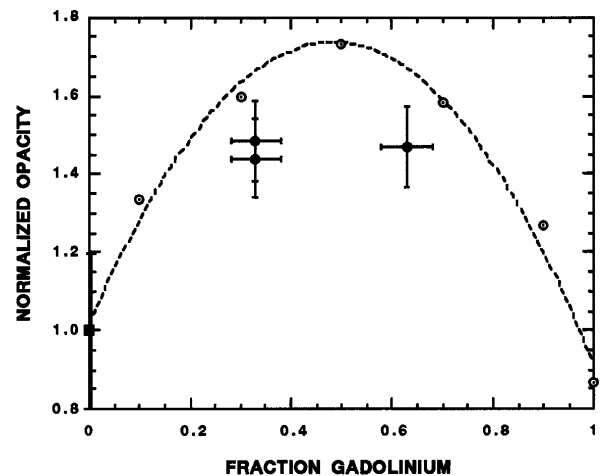

FIG. 4. Rosseland mean opacity of composite normalized to that of pure Au at a temperature of 250 eV and a density of 1 g/cm^2. The open points correspond to the results of XSN calculations, and the line is a quadratic fit to those points. The solid points show the normalized opacity of the measurements as determined using Eq. (4). The datum at zero concentration of Gd corresponds to earlier work that verified the XSN opacity model.

In addition, the measured concentration of Gd is precise to about $\pm 5\%$.

The solid curve in Fig. 4 shows the calculated Rosseland mean opacity of the Au/Gd mixture as a function of Gd concentration using the XSN opacity model [11] and assuming a temperature of 250 eV and a density of 1.0 g/cm². These calculations indicate the maximum improvement in opacity corresponds to a 50/50 mixture of Au and Gd. The overall improvement in the opacity (over that of pure Au at the same temperature and density) is a factor of 1.7. This curve is normalized to the Rosseland mean opacity of Au at 1.0 g/cm³ and a temperature of 250 eV [κ_R(Au) = 1500 cm²/g]. The opacity of Gd at this temperature and density is 1300 cm²/g. An independent series of experiments [13] measured Marshak wave propagation through different thicknesses of Au foil ($1-3 \mu$m) and monitored the radiation at two different energies (225 and 550 eV). In these experiments the hohlraum temperatures were 250 to 265 eV and they validated the XSN opacity model to within 20% for Au at these temperatures. We indicate the results of those experiments by the datum at the pure Au end of the curve (fraction Gd = 0).

The opacity calculation shown in Fig. 4 represents one specific density and temperature; in reality, the experiment samples a range of densities and temperatures. In view of the relative simplicity of the model to the actual complicated time-dependent phenomenon, the model is remarkably accurate in that the measurements as interpreted by the model are only about 10% to 12% lower than the XSN calculation. Perhaps an even more sophisticated treatment of bound-bound transitions than XSN employs would account for the discrepancy. The most accurate way to determine the opacity of the composite is to simulate the experiment with a rad-hydro code such as LASNEX. We are using this code to study the transport of radiation through materials with the same composition as that used in the experiment. A frequency dependent radiation source corresponding to a 250-eV radiation temperature is applied to the various samples. We then "observe" the breakout of the radiation on the back side of the sample, just as in the experiment. These calculations give a ratio of 1.3 for the burnthrough times in a 250-eV channel for a 2:1 Au/Gd mixture, as opposed to the measured 1.2, and a ratio of 1.25 for a 1:2 Au/Gd mixture compared with a measured value of 1.3. Thus, the burnthrough times are in reasonable agreement with the experiment. More detailed calculations are ongoing. In addition, we are investigating different concentrations of Au/Gd to determine more precisely the effect of the Gd on the Au opacity.

We have demonstrated that by combining the appropriate elements we can produce a composite whose Rosseland mean opacity is higher than that of either of the constituents at a given temperature and density. The elements must be chosen so that the high-opacity regions of one element overlap with the low-opacity regions of the other. Because the composites have a higher reemission coefficient to the incident radiation, less energy is lost to the wall. For example in the scale-1 hohlraums used in these experiments the wall losses account for about 75% of the total energy lost (the remainder going out the laser entrance holes; there are no capsule losses in these empty hohlraums). The observed 50% increase in the wall opacity results in a 15% reduction in wall loss and results in 12% less energy required to achieve the same hohlraum temperature. Alternatively, the same amount of laser energy leads to an increase in temperature of about 8 eV (about 12% more flux available to drive a capsule).

*Present address: Sandia National Laboratory, P.O. Box 5800, Albuquerque, NM 87185.

[1] J. D. Lindl, R. L. McCrory, and E. M. Campbell, Phys. Today **45**, No. 9, 32 (1992).

[2] J. H. Nuckolls, L. Wood, A. Thiessen, and G. B. Zimmerman, Nature (London) **239**, 129 (1972).

[3] John Lindl, Phys. Plasmas **2**, 3933 (1995).

[4] J. D. Lindl, R. O. Bangerster, J. W.-K. Mark, and Y. L. Pan, in *Heavy Ion Inertial Fusion,* edited by Martin Reiser, Terry Godlove, and Roger Bangerster, AIP Conf. Proc. No. 152 (AIP, New York, 1986).

[5] M. D. Rosen, Lawrence Livermore National Laboratory Report No. UCRL-50055-97, 1979 (unpublished).

[6] M. D. Rosen, Lawrence Livermore National Laboratory Report No. UCRL-ID 121585, 1995 (to be published).

[7] R. Pakula and R. Sigel, Phys. Fluids **28**, 232 (1985); **29**, 1340(E) (1986).

[8] R. E. Marshak, Phys. Fluids **1**, 24 (1958).

[9] S. Rosseland, Mon. Not. R. Astron. Soc. **84**, No. 7, 525 (1924).

[10] Jon T. Larsen, in *Radiative Properties of Hot Dense Matter: Proceedings of the 4th International Workshop,* edited by W. Goldstein, C. Hooper, J. Gauthier, J. Seely, and R. Lee (World Scientific, Singapore, 1990).

[11] W. A. Lokke and W. H. Grasberger, Lawrence Livermore National Laboratory Report No. UCRL-52276, 1977 (unpublished).

[12] R. Sigel *et al.,* Phys. Rev. Lett. **65**, 587 (1990).

[13] J. L. Porter and A. R. Thiessen, Lawrence Livermore National Laboratory Report No. CLY-92-059, 1992 (unpublished).

[14] V. J. L. White, J. M. Foster, J. C. V. Hansom, and P. A. Rosen, Phys. Rev. E **49**, R4803 (1994).

[15] F. Ze *et al.,* J. Appl. Phys. **66**, 1935 (1989).

[16] R. L. Kauffman *et al.,* Phys. Rev. Lett. **73**, 2320 (1994).

[17] H. N. Kornblum, R. L. Kauffman, and J. A. Smith, Rev. Sci. Instrum. **57**, 2179 (1986).